Draft version September 5, 2022
Typeset using LaTeX **twocolumn** style in AASTeX631

arXiv:2208.01673v2 [astro-ph.GA] 2 Sep 2022

Unveiling the contribution of Pop III stars in primeval galaxies at redshift ≥ 6

Shafqat Riaz,[1] Tilman Hartwig,[2,3,4] and Muhammad A. Latif[5]

[1] *Center for Field Theory and Particle Physics and Department of Physics, Fudan University, 200438 Shanghai, China*
[2] *Institute for Physics of Intelligence, School of Science, The University of Tokyo, Bunkyo, Tokyo 113-0033, Japan*
[3] *Department of Physics, School of Science, The University of Tokyo, Bunkyo, Tokyo 113-0033, Japan*
[4] *Kavli Institute for the Physics and Mathematics of the Universe (WPI), The University of Tokyo Institutes for Advanced Study, The University of Tokyo, Kashiwa, Chiba 277-8583, Japan*
[5] *Physics Department, College of Science, United Arab Emirates University, PO Box 15551, Al-Ain, UAE*

ABSTRACT

Detection of the first stars has remained elusive so-far but their presence may soon be unveiled by upcoming JWST observations. Previous studies have not investigated the entire possible range of halo masses and redshifts which may help in their detection. Motivated by the prospects of detecting galaxies up to $z \sim 20$ in JWST early data release, we quantify the contribution of Pop III stars to high-redshift galaxies from $6 \leq z \leq 30$ by employing the semi-analytical model a-sloth, which self-consistently models the formation of Pop III and Pop II stars along with their feedback. Our results suggest that the contribution of Pop III stars is the highest in low-mass halos of $10^7 - 10^9$ $M_\odot$. While high-mass halos $\geq 10^{10}$ $M_\odot$ contain less than 1% Pop III stars, they host galaxies with stellar masses of 10^9 $M_\odot$ as early as $z \sim 30$. Interestingly, the apparent magnitude of Pop III populations gets brighter towards higher redshift due to the higher stellar masses, but Pop III-dominated galaxies are too faint to be directly detected with JWST. Our results predict JWST can detect galaxies up to $z \sim 30$, which may help in constraining the IMF of Pop III stars and will guide observers to discern the contribution of Pop III stars to high-redshift galaxies.

Keywords: Population III stars (1285) — Population II stars (1284) — High-redshift galaxies (734) — James Webb Space Telescope (2291)

1. INTRODUCTION

Tremendous progress on the observational frontier has enabled astronomers to detect galaxies up to the cosmic dawn during the past two decades. About thousand galaxies have been detected detected at z >6 (Bouwens et al. 2016; Oesch et al. 2016; Harikane et al. 2022; Schaerer et al. 2022; Finkelstein et al. 2022) with candidates up to z$\sim$ 20 being revealed in James Webb space telescope (JWST) early data release (Carnall et al. 2022; Castellano et al. 2022; Naidu et al. 2022; Yan et al. 2022; Adams et al. 2022), which may just be the tip of the iceberg (Dayal & Ferrara 2018). One of the primary goals of JWST is to unveil primeval galaxies that contain Pop III stars and revolutionize our understanding of the high-redshift universe. In fact, the commissioning of JWST has shown that unprecedented sensitivity of NIRCam can detect objects with a flux of ~ 10 nJy (equivalent to apparent magnitude of ~ 29) at SNR$= 10$ for a standard exposure time of 10 ks (Rigby et al. 2022). With longer exposure times and gravitational lensing, JWST may discover even more and fainter galaxies at redshift > 10. Therefore, it is very timely to make predictions about the contribution and presence of Pop III stars. Such work will help in guiding forthcoming JWST observations.

Pop III stars are expected to form in pristine minihalos of a few times 10^6 $M_\odot$ at z ≥ 10 (Skinner & Wise 2020; Schauer et al. 2021). They ushered the universe out of cosmic dark ages, initiated the process of re-ionization and shaped the formation of high-redshift galaxies via their feedback. Depending on their mass, they are expected to have short lifetimes, may go off as a supernovae (SNe) and enrich the surrounding ISM with metals (Heger & Woosley 2002). In the aftermath of Pop

Corresponding author: Muhammad A. Latif
latifne@gmail.com

III SNe, second generation stars known as Pop II stars form from metal-enriched gas with metallicity as low as $\geq 10^{-5}$ $Z_\odot$ (Schneider et al. 2003; Omukai et al. 2005). Recent, numerical simulations including UV radiative feedback from stars suggest Pop III characteristic masses of a few ten of $M_\odot$ (Clark et al. 2011; Stacy et al. 2016; Sugimura et al. 2020; Latif et al. 2022) substantially lower than previously thought (Bromm et al. 2002; Abel et al. 2002; Yoshida et al. 2008). However, direct observations are required to constrain their mass spectrum, which might be achieved with upcoming observations of high-redshift galaxies with JWST.

In fact, the star formation rate density (SFRD) of Pop III stars dominates at $z \geq 15$ (Hartwig et al. 2022) suggesting their significant role in shaping high-redshift galaxies and the necessity of taking into account the contribution of Pop III stars in modeling their SEDs. Zackrisson et al. (2011, 2017) investigated the spectral evolution of first galaxies finding that Pop III galaxies with stellar masses as low as $10^5\,M_\odot$ can be detected at z $\sim$ 10 and discussed various observational strategies. Renaissance simulations have examined the properties of high-redshift galaxies such as their stellar masses, SFRs, UV luminosity functions and escape fractions of ionizing radiation (O'Shea et al. 2015; Xu et al. 2016). Their results suggest that large fractions of Pop III stars may remain elusive to direct detection at z=15 (Barrow et al. 2018). Jaacks et al. (2019) studied the legacy of Pop III star formation and found that the Pop III contribution to SFRDs significantly increases beyond z$\sim$15 up to 50% while their contribution to ionizing emissivity is about 60 %. Recently, Katz et al. (2022) simulated a halo of $3 \times 10^8\,M_\odot$ at z=10 to investigate the possibility of Pop III detection with JWST and found that key signatures of Pop III stars fade away quickly due to their short lifetimes. These studies could not investigate the entire range of possible halo masses and redshifts due to numerical limitations, but they indicate that Pop III stars might be detectable at high redshift.

Motivated by the prospects of detecting galaxies with JWST up to z $\sim$ 20 (Yan et al. 2022), in this letter, we perform a comprehensive study which self-consistently models the formation of both Pop III & Pop II stars along with their chemical, mechanical and radiative feedback for a statistical sample of high-redshift galaxies. We simulate here a wide range of galaxies forming in different halo masses at $z = 6 - 30$ because of the expected dominance of Pop III stars in this era and report their properties, such as masses and luminosities for Pop III and Pop II stars. These results will help to identify the possible contributions of Pop III stars in the upcoming data of JWST.

2. METHODOLOGY

We use the semi-analytical model A-SLOTH to simulate the formation of the first galaxies (Hartwig et al. 2022; Magg et al. 2022). The model is based on dark matter merger trees, which are generated with the Extended Press-Schechter formalism (EPS, Press & Schechter 1974; Bond et al. 1991). Given a halo mass and final redshift, the code first generates a dark matter merger tree backwards in time and then simulates the baryonic physics and feedback forward in time. Stars form once a halo is above the critical mass for efficient gas cooling (Schauer et al. 2021), which includes the baryonic streaming velocity and a Lyman-Werner background, following Hartwig et al. (2022). A-SLOTH includes chemical, radiative, and mechanical feedback from stars and different types of SNe and distinguishes between Pop III and Pop II star formation based on the ISM composition (Chiaki et al. 2017), which results in an effective threshold metalliticty of around $10^{-5}\,Z_\odot$.

We sample individual stars based on pre-defined initial mass functions (IMFs) for Pop III and Pop II stars. This allows us to trace the lifetime and feedback of stars and their supernova explosions accurately in time. Moreover, we can precisely determine the surviving stellar mass at any redshift based on their lifetimes. Hence, our model does not rely on analytical star formation histories, or assumes a single stellar population. Instead, we model the formation of individual stars in high-redshift galaxies self-consistently.

The model is calibrated based on six observables, such as the ionization history and the cosmic SFRD, which guarantees reliable predictions up to high redshifts. For Pop II stars, we assume a Kroupa IMF in the mass range 0.1-100 $M_\odot$while for Pop III stars we employ a logarithmically flat IMF in the mass range $5 - 210\,M_\odot$, which best reproduces observations (Hartwig et al. 2022). However, the lower-mass end of the Pop III IMF is poorly constrained and for this research we allow Pop III stars to form down to $3\,M_\odot$. This does not change the global properties of the model, but it allows us to show more fine-grained results due to their slightly longer lifetimes.

A-SLOTH resolves minihalos with $M_h \geq 10^6\,M_\odot$ at the highest redshifts. While this high mass resolution is excellent to follow the physics accurately, such small galaxies might suffer from stochastic sampling effects because they only contain a handful of stars. Therefore, we resample each galaxy several times with different random seeds and report the median value and the central 68% percentile to quantify the cosmic variance.

3. RESULTS

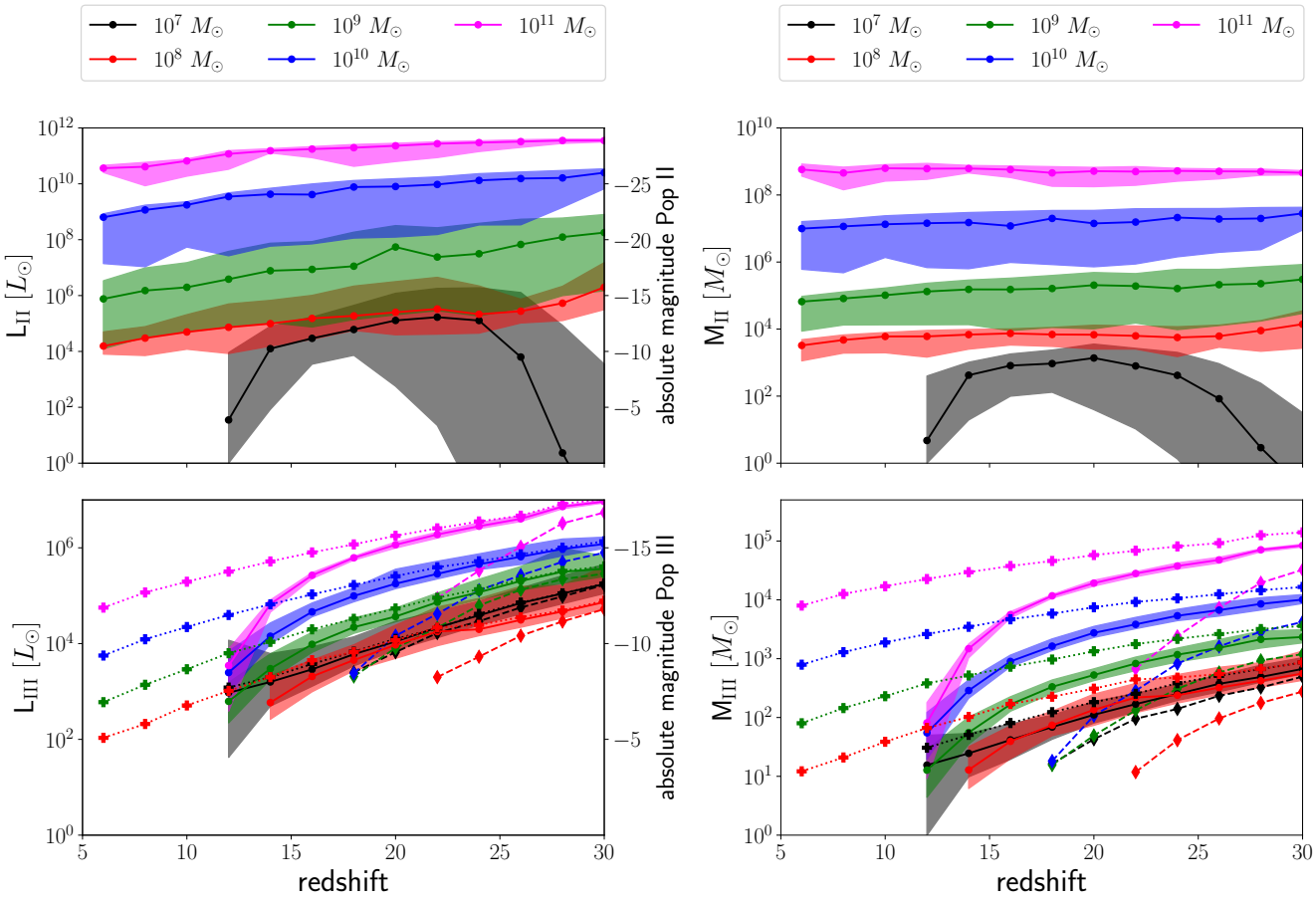


Figure 1. Luminosities, absolute magnitudes (left panels) and stellar masses (right panels) of both Pop II & Pop III stars surviving until the respective redshift are shown in the top and the bottom panels, respectively. In the bottom panels plus signs (dotted lines) and diamonds (dashed lines) are for M_{min} = 0.8 and 5 $M_\odot$, respectively. In each panel, the filled color region represents the central 68 percent cosmic variance.

We have simulated a large number of high-redshift galaxies using A-SLOTH, which allows to self-consistently model the formation of Pop III and Pop II stars. Moreover, we have explored a variety of halos with masses ranging from $10^7 - 10^{11}$ $M_\odot$ from z = 30 down to z = 6. To mimic cosmic stochasticity, each combination of redshift and halo mass is simulated about 100 times. This comprehensive study enables us to estimate the properties of high-redshift galaxies such as stellar masses, star formation rates, metallicities, luminosities and to quantify the relative contribution of Pop III stars.

The average Pop III stellar mass varies from $10 - 10^5$ $M_\odot$ for halos of $10^7 - 10^{11}$ $M_\odot$ and increases with redshift, see Fig. 1. At $z \leq 10$, Pop III stars form only in $< 25\%$ of simulated halos due to metal pollution. The Pop II stellar mass varies from $100 - 10^9$ $M_\odot$ for $10^7 - 10^{11}$ $M_\odot$ halos. Overall, the Pop II stellar mass does not significantly change in similar mass halos from z = 30 − 6 as shown in Fig. 1. Statistical variations in Pop III stellar mass from halo to halo are within a factor of a few and prominent in low-mass halos as they are more prone to stellar feedback and effects from random sampling.

We have selected here a fudicial value of $M_{min} = 3\,M_\odot$ for the lower cutoff mass which is the logarithmic mean of the possible range of minimum Pop III stellar masses between $0.8 - 10\,M_\odot$ (Hartwig et al. 2022) and therefore the most representative value. We also investigated the impact of lower cutoff masses on the survival of Pop III stars. Our findings suggest that for a cutoff mass of $5\,M_\odot$, Pop III stars stop contributing already at z=18 but for lower cutoff mass of $0.8\,M_\odot$ they can survive down to z ∼ 6. Overall, for the lowest cutoff mass, the Pop III stellar mass is a factor of few higher than our fiducial case at all redshifts.

Typical luminosity of Pop III stellar populations varies from $10^3 - 10^7$ $L_\odot$ while for Pop II it ranges from $10^3 - 10^{12}$ $L_\odot$ as depicted in Fig. 1. Both Pop III & Pop

II luminosities increase with redshift and are highest at z $\sim$ 30. For high-mass halos, the Pop III luminosity is a few orders of magnitude smaller than Pop II, but for halos with masses $10^7 - 10^8$ $M_\odot$, the Pop III luminosity is roughly comparable to Pop II. These results suggest that some massive galaxies with stellar mass of 10^9 $M_\odot$ at z > 15 have luminosities of 10^{12} $L_\odot$ and are as bright as their counterparts at z $\sim$ 10 (Naidu et al. 2022).

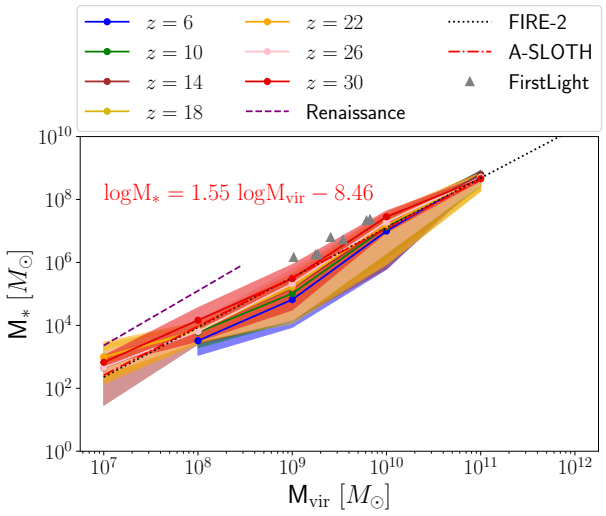


Figure 2. Stellar mass ($M_* = M_{II} + M_{III}$) vs halo virial mass (M_{vir}) for redshifts between $6 - 30$. Stellar mass consists of both Pop II & Pop III stars that have survived until the respective redshift. The solid lines represent the median derived from A-SLOTH with different random seeds and the colored region shows the central 68 percentile variance. The red dash-dotted line and formula show a linear fit to our data. It is in very good agreement with the results from the FIRE-2 simulation (Ma et al. 2018). The gray triangles represent data from the First Light simulation at $z = 9.6$ (Ceverino et al. 2017) and the dashed purple line depicts the fit taken from the Renaissance simulation (O'Shea et al. 2015).

Our estimates for stellar mass vs halo mass for the entire sample of galaxies from z = 30 − 6 are shown in Fig. 2. Total stellar mass varies from $\sim 10^2$ to 10^9 $M_\odot$ for halo masses of $10^7 - 10^{11}$ $M_\odot$ and monotonically increases with halo mass. Scatter in the plot is due to the statistical variations in the merger trees and IMF sampling. We find no statistically significant change in the stellar mass to halo mass relation in the redshift range $6 \leq z \leq 30$, i.e., the results at all redshifts lie within their uncertainty range. Overall, our results are in good agreement with previous studies (O'Shea et al. 2015; Ceverino et al. 2017; Ma et al. 2018; Jaacks et al. 2019; Pallottini et al. 2022). However, the Renaissance simulation predicts more stars at a given halo mass, which according to Ceverino et al. (2017) is due to the inefficient feedback.

To further elucidate the contribution of Pop III stars to high-redshift galaxies, we show the ratios of Pop III to total stellar mass and Pop III to total luminosity in Fig. 3. It shows that contribution of Pop III stars is close to unity at z > 25 and highest in low-mass halos at all times from z=30 down to z=10. This contribution drops to below 1% for halos of $\geq 10^{10}$ $M_\odot$. Furthermore, statistical variations in the Pop III contribution to high-redshift galaxies are two orders of magnitude. Our findings suggest that low-mass galaxies forming at z $\geq$ 12 are the best targets to find Pop III stars. The contribution of Pop III stars in high-mass galaxies is much lower than Pop II stars which may pose a challenge to identify them.

To compare our results with observations, we estimated the bolometric apparent magnitudes of our galaxies and their statistical variations, which are shown in Fig. 4. To calculate the bolometric apparent magnitude, we used $m = -26.83 - 2.5 \log(F/F_\odot)$, where $F_\odot$ is the Solar flux, and F is the flux of our simulated galaxy, which is estimated using the luminosity distance relation for a given redshift. We compute the luminosities of Pop III & Pop II stars separately. For Pop III stars, we use the fitting function given in Eq 3 of Windhorst et al. (2018) while for Pop II stars, we use a standard luminosity-mass relation. We also show the expected apparent magnitude of Pop III and Pop II stars separately that enables us to quantify their contributions and compare them with the detection limit of JWST. The apparent magnitude of Pop III stars varies from 40-50, increases with redshift, and is brightest for a 10^{11} $M_\odot$ halo at z $\sim$ 30, much fainter than the JWST detection limit of 29.2. The range of apparent magnitude for Pop II stars varies from 27-50, which is much larger than for Pop III stars, but only the most massive galaxy will be visible to JWST. In fact, such a galaxy can be detected as early as z=30.

We further show the fraction of Pop III luminosity against the total luminosity/AB magnitude for the entire sample of simulated galaxies in Fig. 5. This figure provides a convenient way to estimate the relative contribution of Pop III stars to the total luminosity of newly detected galaxies at high redshift. It is found that faint galaxies with AB magnitude below -20 are the best candidates for finding Pop III stars across all redshifts but are well below the detection limits of JWST. The brightest galaxies contain less than 1% Pop III stars but their AB magnitudes are within the range of JWST even at z=30. Based on the halo mass function of Warren et al. (2006), the expected number density of such galaxies is

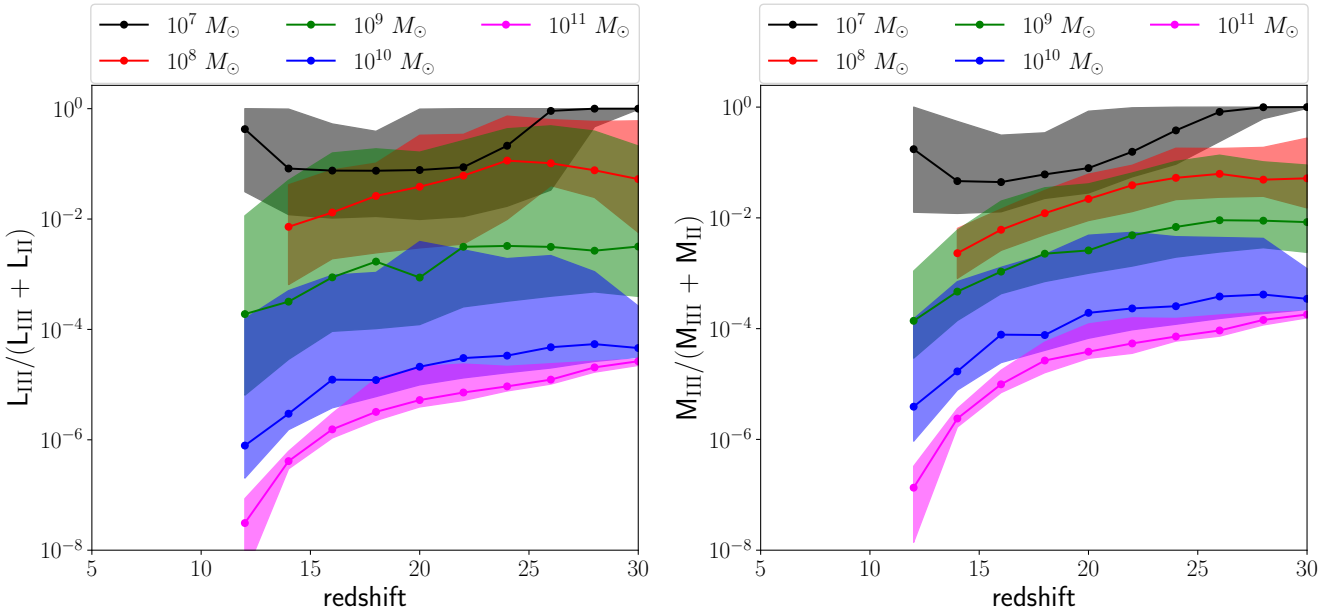


Figure 3. The fractions of Pop III luminosity (left panel) and stellar mass (right panel) for our simulated galaxies are shown as a function of redshift. The halo mass varies from $10^7 - 10^{11}\ M_\odot$ and the colored region represents the central 68 percentile variance.

≤ 1 per Gpc^3 at z=26. Therefore, these galaxies are expected to be rare at earlier times. Nevertheless, we expect such galaxies can be unveiled in upcoming wide survey JWST observations.

4. DISCUSSION AND CONCLUSIONS

We have simulated a large ensemble of high-redshift galaxies using the semi-analytical model A-SLOTH, which has been calibrated against six independent observables and simultaneously models both Pop III & Pop II stellar populations along with their feedback. This unique sample of galaxies allowed us to study the statistical variations among the properties of high-redshift galaxies, such as stellar masses, luminosities, star formation rates, fraction and contribution of Pop III stars to their host galaxies. Our results suggest that best candidates to search for Pop III stars are low-mass galaxies from $10 \leq z \leq 30$ which are challenging to be detected with JWST and the contribution of Pop III stars decreases to less than 1 % in massive galaxies. We further predict that JWST can detect galaxies up to $z \sim 30$ as their AB magnitudes lie within its range. These findings may guide observers in planning their observations and also help to improve spectral modeling of high-redshift galaxies.

We consider the impact of both baryonic streaming motions and LW radiation based on Schauer et al. (2021), which increase the halo threshold mass above $10^6\,M_\odot$. Therefore, Pop III stars cannot form in halos with masses lower than this at $z < 20$. Pop III stars can still form in halos of a few times $10^6\,M_\odot$ at $z > 20$. They have typical masses of about $10^3\,M_\odot$ but their feedback limits the formation of Pop II stars in the host halos. Interestingly, these halos hosting very young Pop III star may be directly detected with ULT in future.

We also investigated the role of the Pop III IMF on our findings by varying its slope from logarithmically flat to Salpeter and found that it has negligible impact on the number of Pop III survivors and total stellar mass. Furthermore, we found that the low cutoff mass of Pop III IMF influences the number of Pop III survivors as well as their masses. We find that Pop III stars can only survive to $z \sim 6$ if their low cutoff mass is $< 3\ M_\odot$ otherwise they die on relatively short timescales and may not survive to such redshifts. Higher cutoff mass ($5\,M_\odot$) decreases the number of Pop III survivors. These results suggest that finding Pop III survivors at $z \leq 10$ may help in constraining the lower mass end of the Pop III IMF.

Our results are in agreement with previous works, which simulated only a limited number of high-redshift galaxies (see Fig. 2). In addition, Barrow et al. (2018) find similar Pop III stellar masses at a given halo mass in the Renaissance simulation. They also report the fraction of Pop III stellar mass to be in the range $10^{-6} - 0.3$ for halos of $10^7 - 10^{10}\,M_\odot$, similar to our results. Recently, Yan et al. (2022) report the discovery of three galaxy candidates with a photometric red-

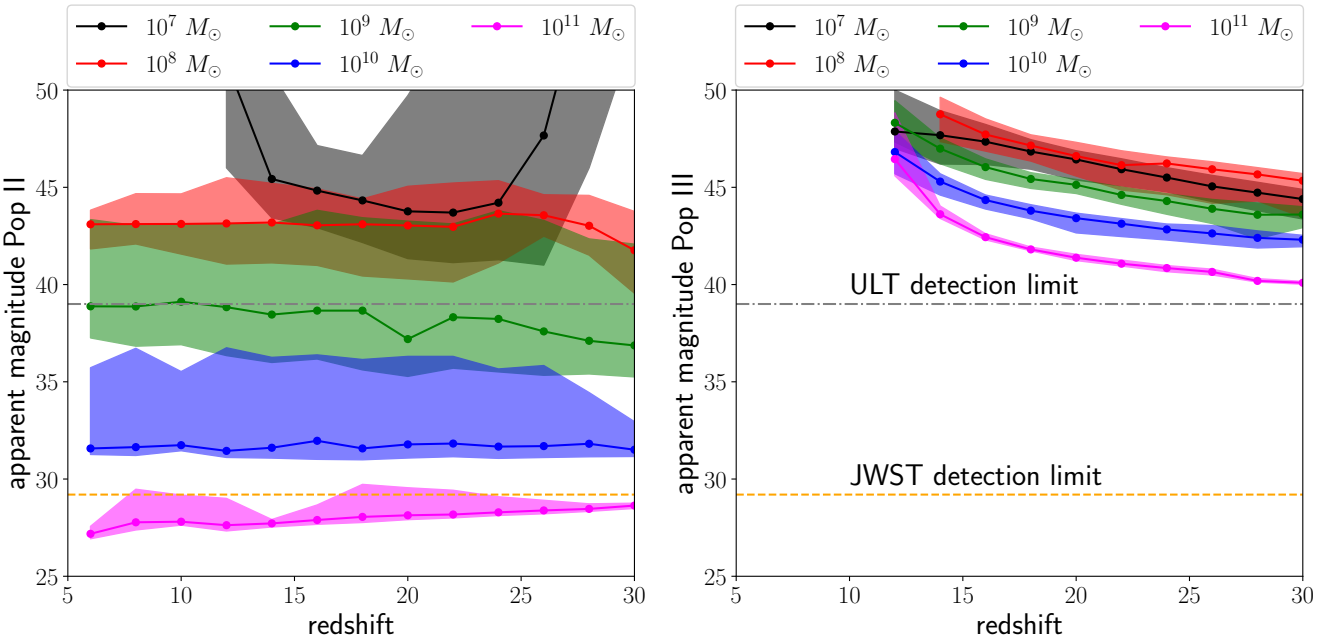


Figure 4. The apparent magnitude of Pop II (left panel) and Pop III (right panel) stars that survived until given redshift as a function of redshift. The halo mass ranges from $10^7 - 10^{11}\ M_\odot$. The orange dashed line in both panels denotes the JWST apparent magnitude limit of 29.2 (SNR=10 for an exposure time of 10 ks in F277W, Rigby et al. 2022). The colored region quantifies the central 68 percentile variance. In the both panels, the gray line at the apparent magnitude of 39 represents the detection limit of Moon-based near-infrared mission, The Ultimately Large Telescope (ULT), proposed in Schauer et al. (2020).

shift of $z \sim 20$ with JWST. These galaxies have stellar masses of $\sim 10^8\,M_\odot$. Based on our results, we can estimate the dark matter halo mass of such galaxies to be $10^{10} - 10^{11}\,M_\odot$ (Fig. 2). This allows us to estimate the contribution of Pop III stars to the bolometric luminosities of such objects to be only $\lesssim 10^{-3}$ (Fig. 3). The contribution of Pop III stars to the luminosity of such objects is hence negligible.

In this work, we employed the stochastic feedback model of A-SLOTH which is based on the EPS merger trees. Although this stochastic feedback is sufficiently accurate (Hartwig et al. 2022), future studies can improve by using A-SLOTH's spatial feedback model based on merger trees extracted from N-body simulations to obtain more realistic results. If we were to perform 3D cosmological simulations, which are prohibitively expensive for such a large sample of galaxies, pockets of metal free gas may exist down to lower redshifts due to inhomogeneous mixing of metals. For example, Liu & Bromm (2020) found from cosmological simulations that such pockets of metal free exist even down to z $\sim$ 4 in massive halos of $\geq 10^9\ M_\odot$. Under these conditions, some Pop III stars may form at lower redshifts.

TH acknowledges funding from JSPS KAKENHI Grant Numbers 19K23437 and 20K14464. MAL thanks UAEU for funding via SURE Plus 3835 and UPAR grant No. 31S390.

Software: A-SLOTH (Hartwig et al. 2022; Magg et al. 2022), python (Van Rossum & Drake 2009), numpy (Harris et al. 2020), scipy (Virtanen et al. 2020), matplotlib (Hunter 2007), astropy (Price-Whelan et al. 2018).

REFERENCES

Abel, T., Bryan, G. L., & Norman, M. L. 2002, Science, 295, 93, doi: 10.1126/science.295.5552.93

Adams, N. J., Conselice, C. J., Ferreira, L., et al. 2022, arXiv e-prints, arXiv:2207.11217. https://arxiv.org/abs/2207.11217

Barrow, K. S. S., Wise, J. H., Aykutalp, A., et al. 2018, MNRAS, 474, 2617, doi: 10.1093/mnras/stx2973

Bond, J. R., Cole, S., Efstathiou, G., & Kaiser, N. 1991, ApJ, 379, 440, doi: 10.1086/170520

Bouwens, R. J., Oesch, P. A., Labbé, I., et al. 2016, ApJ, 830, 67, doi: 10.3847/0004-637X/830/2/67

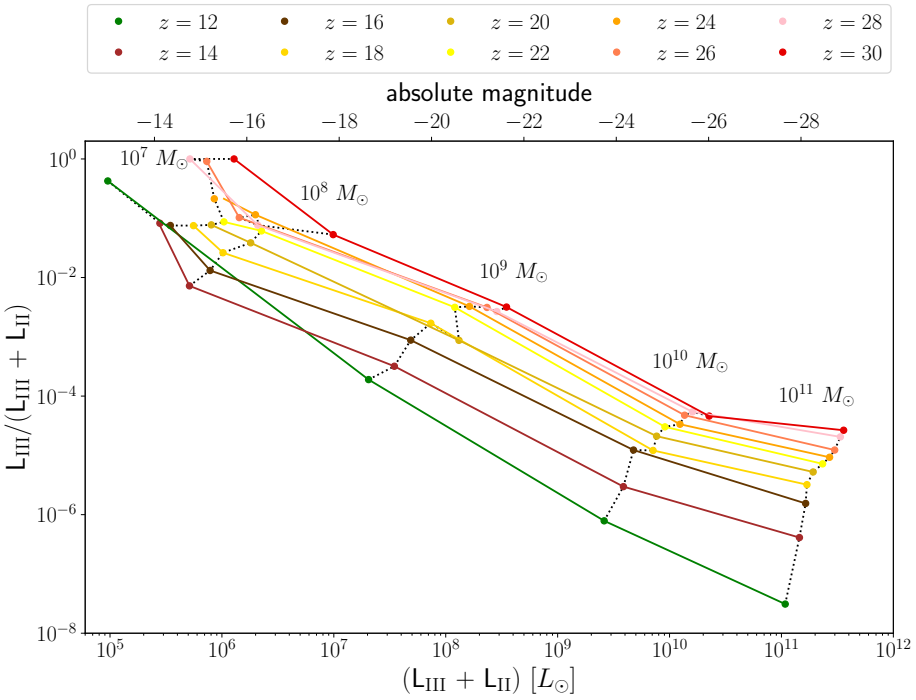


Figure 5. The luminosity fraction of Pop III stars as a function of the total luminosity and absolute magnitude for different halos as depicted above each curve. We consider only the surviving Pop II and Pop III stars at the final redshift. The color of the dot reflects the final redshift and the colored solid line represents the trend in luminosity fraction with increasing halo mass at a given redshift.

Bromm, V., Coppi, P. S., & Larson, R. B. 2002, ApJ, 564, 23, doi: 10.1086/323947

Carnall, A. C., Begley, R., McLeod, D. J., et al. 2022, arXiv e-prints, arXiv:2207.08778. https://arxiv.org/abs/2207.08778

Castellano, M., Fontana, A., Treu, T., et al. 2022, arXiv e-prints, arXiv:2207.09436. https://arxiv.org/abs/2207.09436

Ceverino, D., Glover, S. C. O., & Klessen, R. S. 2017, MNRAS, 470, 2791, doi: 10.1093/mnras/stx1386

Chiaki, G., Tominaga, N., & Nozawa, T. 2017, MNRAS, 472, L115, doi: 10.1093/mnrasl/slx163

Clark, P. C., Glover, S. C. O., Smith, R. J., et al. 2011, Science, 331, 1040, doi: 10.1126/science.1198027

Dayal, P., & Ferrara, A. 2018, PhR, 780, 1, doi: 10.1016/j.physrep.2018.10.002

Finkelstein, S. L., Bagley, M., Song, M., et al. 2022, ApJ, 928, 52, doi: 10.3847/1538-4357/ac3aed

Harikane, Y., Inoue, A. K., Mawatari, K., et al. 2022, ApJ, 929, 1, doi: 10.3847/1538-4357/ac53a9

Harris, C. R., Millman, K. J., van der Walt, S. J., et al. 2020, Nature, 585, 357, doi: 10.1038/s41586-020-2649-2

Hartwig, T., Magg, M., Chen, L.-H., et al. 2022, arXiv e-prints, arXiv:2206.00223. https://arxiv.org/abs/2206.00223

Heger, A., & Woosley, S. E. 2002, ApJ, 567, 532, doi: 10.1086/338487

Hunter, J. D. 2007, Computing in Science & Engineering, 9, 90, doi: 10.1109/MCSE.2007.55

Jaacks, J., Finkelstein, S. L., & Bromm, V. 2019, MNRAS, 488, 2202, doi: 10.1093/mnras/stz1529

Katz, H., Kimm, T., Ellis, R. S., Devriendt, J., & Slyz, A. 2022, arXiv e-prints, arXiv:2207.04751. https://arxiv.org/abs/2207.04751

Latif, M. A., Whalen, D., & Khochfar, S. 2022, ApJ, 925, 28, doi: 10.3847/1538-4357/ac3916

Liu, B., & Bromm, V. 2020, MNRAS, 497, 2839, doi: 10.1093/mnras/staa2143

Ma, X., Hopkins, P. F., Garrison-Kimmel, S., et al. 2018, MNRAS, 478, 1694, doi: 10.1093/mnras/sty1024

Magg, M., Hartwig, T., Chen, L.-H., & Tarumi, Y. 2022, Journal of Open Source Software, 7, 4417, doi: 10.21105/joss.04417

Naidu, R. P., Oesch, P. A., van Dokkum, P., et al. 2022, arXiv e-prints, arXiv:2207.09434. https://arxiv.org/abs/2207.09434

Oesch, P. A., Brammer, G., van Dokkum, P. G., et al. 2016, ApJ, 819, 129, doi: 10.3847/0004-637X/819/2/129

Omukai, K., Tsuribe, T., Schneider, R., & Ferrara, A. 2005, ApJ, 626, 627, doi: 10.1086/429955

O'Shea, B. W., Wise, J. H., Xu, H., & Norman, M. L. 2015, ApJL, 807, L12, doi: 10.1088/2041-8205/807/1/L12

Pallottini, A., Ferrara, A., Gallerani, S., et al. 2022, MNRAS, 513, 5621, doi: 10.1093/mnras/stac1281

Press, W. H., & Schechter, P. 1974, ApJ, 187, 425, doi: 10.1086/152650

Price-Whelan, A. M., Sipőcz, B., Günther, H., et al. 2018, The Astronomical Journal, 156, 123

Rigby, J., et al. 2022, arXiv e-prints, arXiv:2207.05632. https://arxiv.org/abs/2207.05632

Schaerer, D., Marques-Chaves, R., Oesch, P., et al. 2022, arXiv e-prints, arXiv:2207.10034. https://arxiv.org/abs/2207.10034

Schauer, A. T. P., Drory, N., & Bromm, V. 2020, ApJ, 904, 145, doi: 10.3847/1538-4357/abbc0b

Schauer, A. T. P., Glover, S. C. O., Klessen, R. S., & Clark, P. 2021, MNRAS, 507, 1775, doi: 10.1093/mnras/stab1953

Schneider, R., Ferrara, A., Salvaterra, R., Omukai, K., & Bromm, V. 2003, Nature, 422, 869

Skinner, D., & Wise, J. H. 2020, MNRAS, 492, 4386, doi: 10.1093/mnras/staa139

Stacy, A., Bromm, V., & Lee, A. T. 2016, MNRAS, 462, 1307, doi: 10.1093/mnras/stw1728

Sugimura, K., Matsumoto, T., Hosokawa, T., Hirano, S., & Omukai, K. 2020, ApJL, 892, L14, doi: 10.3847/2041-8213/ab7d37

Van Rossum, G., & Drake, F. L. 2009, Python 3 Reference Manual (Scotts Valley, CA: CreateSpace)

Virtanen, P., Gommers, R., Oliphant, T. E., et al. 2020, Nature Methods, 17, 261, doi: 10.1038/s41592-019-0686-2

Warren, M. S., Abazajian, K., Holz, D. E., & Teodoro, L. 2006, ApJ, 646, 881, doi: 10.1086/504962

Windhorst, R. A., Timmes, F. X., Wyithe, J. S. B., et al. 2018, ApJS, 234, 41, doi: 10.3847/1538-4365/aaa760

Xu, H., Wise, J. H., Norman, M. L., Ahn, K., & O'Shea, B. W. 2016, ApJ, 833, 84, doi: 10.3847/1538-4357/833/1/84

Yan, H., Ma, Z., Ling, C., et al. 2022, arXiv e-prints, arXiv:2207.11558. https://arxiv.org/abs/2207.11558

Yoshida, N., Omukai, K., & Hernquist, L. 2008, Science, 321, 669, doi: 10.1126/science.1160259

Zackrisson, E., Rydberg, C.-E., Schaerer, D., Östlin, G., & Tuli, M. 2011, ApJ, 740, 13, doi: 10.1088/0004-637X/740/1/13

Zackrisson, E., Binggeli, C., Finlator, K., et al. 2017, ApJ, 836, 78, doi: 10.3847/1538-4357/836/1/78